Proceedings of the 12th International Symposium on Physics of Materials, Prague, September 4–8, 2011

Effect of Si and Fe on the Recrystallization Response of Al–Mn Alloys with Zr Addition

M. Karlík[a,*], T. Mánik[a], M. Slámová[b] and H. Lauschmann[a]

[a]Faculty of Nuclear Sciences and Physical Engineering, Department of Materials
Czech Technical University in Prague, Trojanova 13, 120 00 Praha 2, Czech Republic
[b]Research Institute of Metals, Panenské Břežany, 250 70 Odolena Voda, Czech Republic

Al–Mn alloys are often used for the production of automotive heat exchanger fins. During brazing at about 600 °C, recrystallization and grain coarsening resulting in the reduction of the strength and possible buckling of the fin can occur. In order to obtain a good recrystallization resistance, the alloy should contain a dense and homogeneous distribution of second phase particles. The effect of Si and Fe addition on the recrystallization response of Al–Mn–Zr alloys direct-chill cast in the laboratory conditions and twin-roll cast in the industrial conditions was examined. Microstructure of the alloys was characterized during downstream processing. The particles were analyzed by light metallography, energy dispersive X-ray spectroscopy and by means of electron backscattering diffraction. Computer assisted quantitative particle analysis was carried out on field emission gun–scanning electron microscope micrographs. Vickers hardness and electrical conductivity were measured at thicker sheets, while at the final gauge of 65 μm the 0.2% proof stress was evaluated. The best recrystallization resistance had twin-roll cast alloy containing 0.5 wt% Si and 0.2 wt% Fe.

PACS: 81.40.−z, 81.05.Bx, 81.70.−q

1. Introduction

Al–Mn alloys are used for the production of the fins of automotive heat exchangers. Recently, the thickness of fins was reduced below 0.1 mm. At this very low thickness, the fin has to maintain its mechanical strength to avoid collapse [1], and at the same time the material should resist recrystallization to keep its strength after brazing at about 600 °C. Therefore, the alloy should contain a dense distribution of second phase particles to exert a drag force (the Zener drag) on moving subgrain and grain boundaries [2]. The best anti-recrystallization addition is scandium, leading to the formation of Al_3Sc dispersoids [3]. However, scandium is very expensive and its commercial use is thus limited. Consequently, Zr addition, resulting in the formation of the Al_3Zr phase, should be used [4–6].

The decomposition of the supersaturated solid solution in pure Al–Mn binary alloys is very slow [7, 8]. The commercial aluminium alloys contain Si and Fe, and these elements can in some cases deteriorate or improve their properties. Additions of iron and silicon decrease the solubility of Mn and speed up the precipitation of Mn-bearing dispersoids, Al_6(Fe,Mn) or α-Al_{12}(Mn,Fe)$_3$Si [7–10]. Furthermore, in Zr-containing alloys Fe and Si support the formation of Al_3Zr particles, because Al_3Zr dispersoids usually precipitate on Si and Fe atom clusters [4]. In addition, Si has also a positive effect on Al_3Zr stability. It substitutes Al in the $D0_{22}$ compound $(Al_{0.72}Si_{0.28})_3Zr$ which is more stable than $D0_{23}$ or $L1_2$ crystal structures [11]. A problem of using Zr as anti-recrystallization addition is that Zr is usually heterogeneously distributed due to the segregation during casting and its low diffusivity [6]. A more homogeneous distribution of Al_3Zr particles could be achieved by two-step precipitation annealing [5, 12]. The size and distribution of dispersoids have a fundamental role also in the regulation of the microstructure of Al–Mn alloys during downstream processing.

Besides small Al_3Zr particles and large primary constituent phases formed during solidification, Al–Mn alloys contain medium sized dispersoids precipitated during heat treatment. These Mn-containing second phase particles (Al_6(Fe,Mn) or α-Al_{12}(Mn,Fe)$_3$Si) can either stimulate or impede grain growth during thermomechanical treatment. Coarse particles (> 1.5 μm) stimulate recrystallization by particle stimulated nucleation (PSN) mechanism [5], smaller particles (< 0.5 μm) assist Al_3Zr dispersoid in impeding the movement of subgrain and grain boundaries [2].

The paper reviews main results of the studies of the influence of Si and Fe on the size and formation of dispersoids and recrystallization behaviour of Al–Mn–Zr alloys prepared by direct-chill (DC) casting in the laboratory conditions [13] and also by twin-roll casting (TRC) in the industrial conditions [14].

2. Experimental details

2.1. DC-cast alloys

The experimental alloys were produced using an Al–1.43 wt%Mn base alloy by DC casting to billets of the dimensions of 20 mm × 55 mm × 100 mm. The results of the chemical analysis are given in Table. The billets were cold rolled with 89% reduction (equivalent strain $\varepsilon \approx 2.5$) to the thickness of 2 mm. One-step and two-step annealing were applied after cold rolling in order to compare the final microstructure, particularly the homogeneity of the distribution and the density of secondary phase particles. Heating to 450 °C, soaking for

* corresponding author; e-mail: Miroslav.Karlik@fjfi.cvut.cz

12 h at this temperature, and cooling (50 °C/h) were applied during one-step annealing. Two-step annealing involved holding the samples for 10 h at the temperature of 250 °C, heating to 450 °C and soaking for 12 h followed by cooling down at the same rate as in the case of one-step annealing.

TABLE Chemical composition of studied alloys (wt%).

	Alloys	Mn	Zr	Fe	Si	Cu	Zn	Al
DC-cast	Al–Mn	1.52	–	0.01	0.05	–	–	balance
	Al–Mn–Zr	1.39	0.10	0.01	0.08	–	–	balance
	Al–Mn–Zr–Fe	1.44	0.10	0.22	0.06	–	–	balance
	Al–Mn–Zr–Si	1.43	0.10	0.01	0.21	–	–	balance
	Al–Mn–Zr–Si–Fe	1.46	0.10	0.22	0.23	–	–	balance
Twin-roll cast	*A* (Fe)	1.10	0.17	0.32	0.13	0.15	0.10	balance
	B (Si)	1.06	0.17	0.18	0.49	0.13	0.10	balance

2.2. Twin-roll cast alloys

Two industrially twin-roll cast strips, 8.5 mm in thickness, were processed in laboratory conditions. The alloy *A* (Fe) had higher amount of iron (0.32 wt%) while the alloy *B* (Si) contained higher amount of silicon. The content of other elements was nearly the same (Table). After cold rolling with 39% reduction to 5.2 mm thickness (equivalent strain $\varepsilon \approx 0.56$), the samples were subjected to the two-step precipitation annealing mentioned above. Annealed samples were cold rolled with 94% reduction to 0.3 mm thickness (equivalent strain $\varepsilon \approx 3.3$) then recrystallization annealed for 3 h at 550 °C, and cold rolled to the final gauge of 0.065 mm (reduction 78%, equivalent strain $\varepsilon \approx 1.76$). These samples were subjected to isochronal annealing for 6 h in the temperature range from 260 to 400 °C. The recrystallization response was monitored on the values of 0.2% proof stress obtained in the tensile test.

2.3. Materials characterization

The Vickers hardness measurements with 10 kg load (HV10) were carried out in order to determine approximately the onset and the progress of the softening processes, recovery and recrystallization, of DC-cast alloys. The precipitation reactions during annealing and the changes in the solid solution concentrations were monitored by electrical conductivity measurements performed using the Foerster Sigmatest device. The microstructure of all samples was studied by Nikon Epiphot 300 metallographic microscope equipped with the camera Hitachi-HBC 20A. The second phase particles were revealed using a 0.5% solution of hydrofluoric acid in water. The grain structure was visualized in the polarized light after anodizing in the Barker reagent. The precipitate size and density of DC-cast alloys were determined on light micrographs, while for TRC alloys electron micrographs were used. The scanning electron microscope (SEM) FEI Quanta 200 F equipped with the Schottky type field-emission gun (FEG) was operated at 5 kV in the backscattered electron (BSE) signal. From each sample, 20 micrographs at the magnification 5000×, and 20 micrographs at the magnification 50000× were recorded to examine coarse and fine second phase particles, respectively. This number of micrographs enabled to analyse more than 3000 particles at each condition to have a statistically sufficient data set [15]. All sets of micrographs were first normalized to have a constant mean value and standard deviation of brightness and then processed by the software written in Matlab [16], using toolboxes Image Processing and Statistics. Coarser particles in the precipitation annealed samples were analyzed by energy dispersive X-ray spectroscopy (EDXS), and also by electron backscattering diffraction (EBSD) phase analysis according to their crystallographic structure.

3. Results

3.1. Hardness and electrical conductivity of DC-cast alloys

On the sheets cold rolled to 2 mm, hardness and electrical conductivity were measured in the initial condition, and on other samples taken at different points of the annealing curve. The differences between the hardness and the conductivity of the samples subjected to one- and two-step annealing were surprisingly only very small, within the range of the experimental scatter [13].

Therefore, only the results obtained after two-step annealing are presented in Fig. 1 showing the evolution of hardness and electrical conductivity of all five DC-cast alloys as a function of time. For the sake of clarity, the corresponding temperature course is also plotted. For all five alloys, the most important drop of hardness accompanied by a steep increase of electrical conductivity arises during heating up from 250 to 450 °C. In this period, most of the precipitates are formed, and the matrix depletes of the solute atoms. In the following 12 h soaking period, the conductivity slightly increases and the hardness somewhat decreases. If we compare the values in the initial condition, the hardness values are in the order of the amount of alloying elements in the solid solution, i.e., the lowest hardness is for the binary alloy Al–Mn (63 HV10), followed by the ternary one Al–Mn–Zr (67 HV10), quaternary Al–Mn–Zr–Fe (69 HV10), and Al–Mn–Zr–Si (78 HV10), and finally Al–Mn–Zr–Si–Fe (80 HV10) (see also Table). If we take into account only

quaternary alloys, the hardening effect of Si in the solid solution is higher than that of Fe, as expected, because of higher Si solubility.

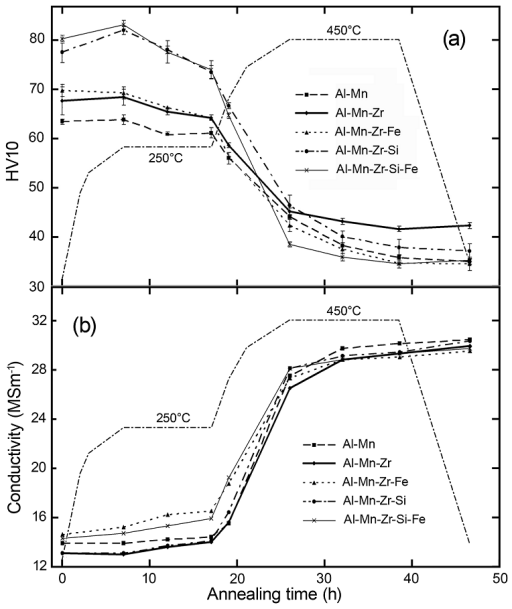

Fig. 1. Evolution of hardness (a) and electrical conductivity (b) of DC-cast alloys subjected to two-step annealing procedure. For the sake of clarity, the corresponding temperature course is also plotted.

Throughout annealing at 250°C, the hardness decreases due to recovery, the important drop of hardness in the middle of the annealing period is due to recrystallization. In the final annealing condition, the hardness of the Al–Mn, Al–Mn–Zr–Fe, and Al–Mn–Zr–Fe–Si is comparable (34 HV10), while the Al–Mn–Zr–Si alloy shows only a small increase (36 HV10) indicating that silicon has a small positive effect on precipitate formation. The highest hardness values not only in the final condition (42 HV10), but also during the whole soaking period, were measured for the Al–Mn–Zr alloy (Fig. 1a). As for the values of the conductivity, the differences between individual alloys are not so important. The values range from 13 to 14 MS m^{-1}, and from 29 to 30.5 MS m^{-1} in the initial and final condition, respectively. More important differences are only in the middle of the annealing period, where the dispersoids precipitate (Fig. 1b).

3.2. Dispersoids in DC-cast alloys

The size and the distribution of the particles during annealing were examined by light microscopy. The micrographs of the particles, corresponding to the surface regions of Al–Mn–Zr, Al–Mn–Zr–Fe, Al–Mn–Zr–Si, and Al–Mn–Zr–Si–Fe sheets in the final condition after two--step annealing and cooling are presented in Fig. 2. The binary alloy is not included since its micrographs were almost the same as those of the Al–Mn–Zr alloy showing a homogeneous distribution of fine particles (Fig. 2a)

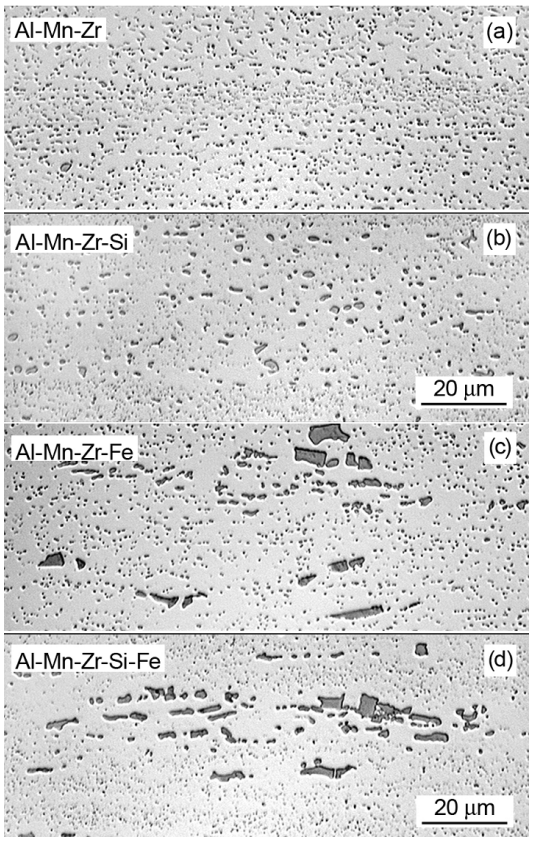

Fig. 2. Micrographs of the particles in surface regions of Al–Mn–Zr, Al–Mn–Zr–Si, Al–Mn–Zr–Fe, and Al–Mn–Zr–Si–Fe DC-cast alloys subjected to two-step annealing. The micrograph of the binary alloy was almost the same as for the Al–Mn–Zr alloy.

through the whole cross-section of the sheet. The addition of Si (Fig. 2b) leads to distinctly coarser particles having a less homogeneous distribution. The alloys with Fe addition (Fig. 2c,d) show coarse primary phases. In the vicinity of these coarse particles, fine secondary precipitate is often absent. The addition of Si and Fe (Fig. 2d) leads to coarse primary phase formation and also to the coarsening of the secondary precipitate. Depleted regions, where fine secondary particles are absent, can be seen not only along the primary phases, but also in other regions at the surface as well as in the middle of the sheet [13].

A quantitative comparison of the particle density in the middle region of the cross-section of the sheets at the final condition for both one- and two-step annealing procedures is in Fig. 3. The density of these relatively coarse (> 0.4 μm) particles decreases with the amount of alloying elements. Another comparison is possible between the one- and two-step annealing. It follows that the two-step annealing yields a higher density of particles in the middle of the sheets, except for the Al–Mn–Zr–Fe alloy (Fig. 3). From the alloys containing Fe, Si or both these elements, the alloy Al–Mn–Zr–Si subjected

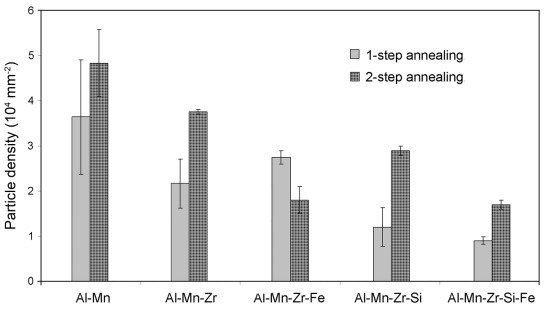

Fig. 3. Density of dispersoids (> 0.4 μm) in DC-cast sheets after one- and two-step annealing.

to the two-step annealing shows the highest density of the precipitates. In consequence, an alloy with higher silicon and lower iron content was selected for the following experiment on industrially twin roll cast alloys. The second alloy contained more iron than silicon to have a reference material for comparison, and also since Al–Mn alloys with excess iron over silicon content were usually used by other authors, e.g. [6, 10, 17].

3.3. Twin-roll cast alloys

Both alloys showed a similar grain structure, typical for twin-roll casting. The grains, 200 to 500 μm long, were inclined from the rolls to the centre of the strip. Besides large blocks (> 30 μm) or needles (> 100 μm long) of the primary Al_3Zr phase present in both alloys, EDXS and EBSD analysis revealed cubic α-$Al_{12}(Mn,Fe)_2Si$ and orthorombic $Al_6(Mn,Fe)$ primary phase in the alloy *A* (Fe), while in the alloy *B* (Si) there was a mixture of cubic α-$Al_{12}(Mn,Fe)_2Si$ and hexagonal α-$Al_{15}(Mn,Fe)_3Si_2$ primary phases.

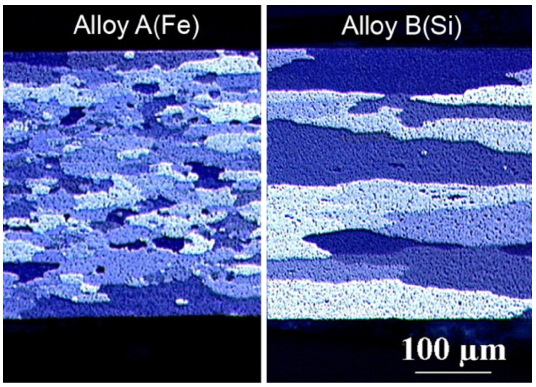

Fig. 4. Light micrographs of the grain structure of twin-roll cast sheets cold rolled to 0.3 mm and annealed for 3 h at 550 °C.

A comparison of the microstructure of the alloys at 0.3 mm thickness after intermediate heat treatment for 3 h at 550 °C is in Fig. 4. Both alloys are fully recrystallized, but their grain structure and particle dispersion are distinctly different. The alloy *A* (Fe) shows very fine

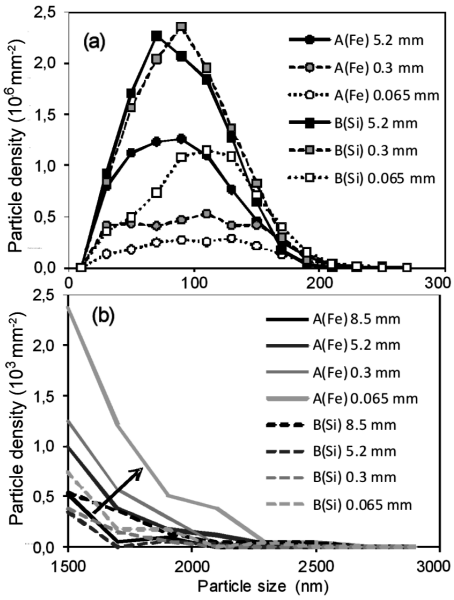

Fig. 5. Distribution of dispersoids during downstream processing of twin-roll cast alloys: (a) fine particles in sheets 5.2, 0.3 and 0.065 mm thick, (b) coarse particles (> 1.5 μm) in sheets 8.5, 5.2, 0.3, and 0.065 mm thick. The arrow in Fig. 5b points out significant increase of density of coarse particles in the alloy *A* (Fe).

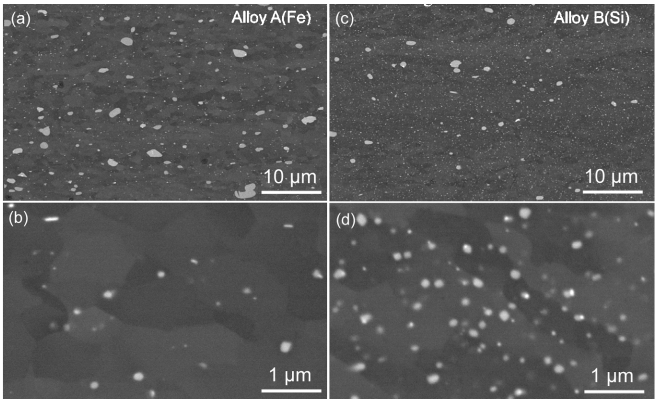

Fig. 6. FEG–SEM micrographs of twin-roll cast alloys at the final gauge of 0.065 mm: (a), (c) coarse particles, (b), (d) fine particles.

grains, 50 to 100 μm long in the centre of the strip, and up to 200 to 300 μm on its surface, while the grains in the alloy *B* (Si) are very coarse, several hundreds of micrometres long. This difference is due to particle stimulated nucleation in alloy *A* (Fe), containing a dense distribution of coarse particles, as it can be noticed on the results of the particle analysis (Fig. 5b). On the other hand, the alloy *B* (Si) contains much lower density of coarse particles which could provoke particle stimulated nucleation. As for fine particles (30 to 200 nm), important for blocking of the movement of subgrain and grain boundaries (the Zener drag), the situation is opposite — their density in

the alloy A (Fe) is much lower than in the alloy B (Si) (Fig. 5a).

FEG–SEM micrographs of the sheets at the final gauge 0.065 mm are in Fig. 6. There is again a distinct difference in the size and distribution of intermetallic particles — they are coarser in the alloy A (Fe) (Fig. 5b, Fig. 6a) and more densely distributed in alloy B (Si) (Fig. 5a, Fig. 6d). The resistance of such microstructures to recrystallization was checked on the evolution of 0.2% proof stress after isochronal annealing for 6 h in the temperature range 260 to 400 °C (Fig. 7). From the sharp decrease in the plots it can be seen that recrystallization of the alloy A (Fe) at these conditions starts at temperatures over 280 °C, while the onset of recrystallization for the alloy B (Si) is shifted to temperatures beyond 350 °C.

4. Discussion

From the results it follows that all alloys containing more than 0.2 wt% Fe (Al–Mn–Zr–Fe, Al–Mn–Zr–Si–Fe and A (Fe) alloys), regardless if they are DC-cast or twin-roll cast, exhibit a higher density of coarser particles (Fig. 2c,d, Fig. 5b, Fig. 6), in whose vicinity the fine secondary precipitate is often absent. In DC-cast alloys, the depleted regions, where fine secondary particles were absent, could be seen not only along the coarsest primary phases, but also in other regions at the surface as well as in the middle of the sheet [13]. On the other hand, the alloys containing more silicon than iron (Al–Mn–Zr–Si, and B (Si)) show lower density of coarse particles (Fig. 2b), and much higher density of fine particles exerting the Zener drag (Fig. 5a). This difference can be attributed to higher silicon content in the solid solution of these alloys, having lower electrical conductivity in the first stages of annealing those Fe-containing alloys (Fig. 1b). As the nucleation of Al_3Zr particles is easier at clusters of Si [4, 11, 18, 19], the higher density of small particles in the alloy B (Si) could be also caused by an increased number of Al_3Zr precipitates more easily nucleated due to a higher silicon concentration in the solid solution of this alloy.

At the cast and intermediate 5.2 mm thickness, the difference in the iron and silicon content of twin-roll cast alloys (alloy A (Fe) 0.32 wt%Fe, 0.13 wt%Si; alloy B (Si) 0.18 wt%Fe, 0.49 wt%Si) had only a negligible influence on the grain size and morphology of the strips. At the cast thickness of 8.5 mm, the coarse particle distribution was also nearly the same (Fig. 5b) (fine particles were not quantified). However, an important difference was in the composition of constituent phases. The alloy A (Fe) with more Fe than Si contained orthorombic $Al_6(Mn,Fe)$ and cubic α-$Al_{12}(Mn,Fe)_2Si$ phases, while in the alloy B (Si) containing more Si, there was a mixture of cubic α-$Al_{12}(Mn,Fe)_2Si$ and hexagonal α-$Al_{15}(Mn,Fe)_3Si_2$ phases. This observation corresponds with the results of Westermann [20], Cama et al. [21], Slámová et al. [22], and Cieslar et al. [23].

During the second step of the precipitation annealing at 450 °C at 5.2 mm thickness, some of the $Al_6(Mn,Fe)$ phase transformed to the cubic alpha phase (6-to-α transformation [17, 24]), but the transformation was not complete and the phase difference between the alloys persisted. This constituent phase difference and higher silicon content in the alloy B (Si) were at the origin of the differentiation of the microstructure and properties during further downstream processing of the alloys.

From the plots in Fig. 5a it follows that the density of small particles after cold rolling from 5.2 to 0.3 mm and annealing 550 °C/3 h in the alloy A (Fe) was substantially reduced, while in the alloy B (Si) it remained almost constant. Therefore, there were several simultaneous processes acting at the same time during this annealing: (i) nucleation of new dispersoids (observed up to the temperature of 500 °C [25]), (ii) 6-to-α transformation and coarsening of dispersoids, and (iii) partial particle dissolution and re-enrichment of the solid solution in Mn and Si [23]. It seems that the dissolution rate and nucleation rate became equal in the alloy B (Si) and so the density of small particles after intermediate annealing 550 °C/3 h remained almost unchanged, while the density of coarse particles increased. On the other hand, in the alloy A (Fe) the coarse particles further coarsened on the expense of the dissolution of the small ones, and there were almost no or much less new dispersoids nucleated.

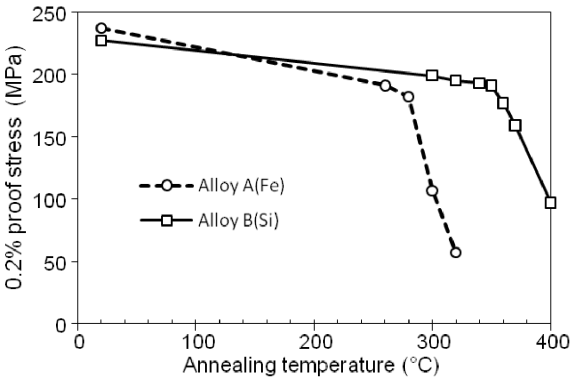

Fig. 7. Evolution of 0.2% proof stress of twin-roll cast foils 0.065 mm thick after annealing for 6 h at given temperature.

If we draw attention to coarse particles (> 1.5 μm), their density in the alloy A (Fe) substantially increased after each thermo-mechanical operation, while the distribution of corresponding particles in the alloy B (Si) did not change significantly (Fig. 5b). The alloy A (Fe) thus more easily recrystallized due to particle stimulated nucleation mechanism (Fig. 4). Its susceptibility to recrystallization was furthermore supported by a low density of small particles (30 to 160 nm), which reduced after precipitation annealing at 5.2 mm thickness with each heat treatment in an important manner (Fig. 5a). In contrast, the density of fine particles in the alloy B (Si) was much higher, it remained almost constant down to the intermediate thickness of 0.3 mm and reduced to a smaller extent at the final thickness (Fig. 5a), therefore exert-

ing an effective dragging force on moving subgrain and grain boundaries. In consequence, the recrystallization resistance of the alloy B (Si) was much higher (Fig. 7).

5. Conclusions

The influence of Si and Fe on the secondary phase particle distribution and recrystallization response of five DC-cast and two industrially twin-roll cast Al–Mn alloys with Zr addition was studied. The main results can be summarized as follows:

1. The density of precipitates in all five DC-cast alloys after one- and two-step annealing was higher in the middle of the 2 mm sheets than in the surface regions. The coarsest primary phases formed in the alloys Al–Mn–Zr–Fe, Al–Mn–Zr–Si–Fe. Close to these coarse particles, fine dispersoids are often absent.

2. The type of the annealing (one-step vs. two-step) practically did not influence the evolution of hardness and electrical conductivity in DC-cast alloys — the differences were only very small. Except for the Al–Mn–Zr–Fe alloy, the two-step annealing procedure led to a higher density of dispersoids in the middle of the sheets than one-step annealing.

3. In the twin-roll cast alloy A (Fe) with excess of iron, the constituent phases were Al_6(Fe,Mn) and cubic α-Al_{12}(Mn,Fe)$_3$Si, while in the alloy B (Si) with higher Si content a mixture of cubic α-Al_{12}(Mn,Fe)$_3$Si and hexagonal α-Al_{15}(Mn,Fe)$_3Si_2$ phases were found. Very coarse blocks or needles of primary Al_3Zr phase were found in both alloys.

4. In the twin-roll cast alloy A (Fe), the density of coarse particles (> 1.5 μm) steadily increased during processing, and at the same time, the density of small precipitates (30 to 160 nm) reduced in an important manner. A (Fe) alloy thus recrystallized easily due to particle stimulated mechanism and insufficient dragging force.

5. On the other hand, in the twin-roll cast alloy B (Si) the distribution of coarse particles did not change significantly, and simultaneously, a high density of fine particles produced by precipitation annealing remained almost constant down to the intermediate thickness of 0.3 mm and reduced to a smaller extent at the final gauge. In consequence, the alloy B (Si) showed much higher recrystallization resistance.

Acknowledgments

This research has been supported by the Czech Ministry of Education, Youth and Sports (project MSM6840770021) and by the Czech Technical University in Prague in the frame of the project SGS 10/301/OHK4/3T/14.

References

[1] A. Kawahara, A. Niikura, T. Doko, *Furukawa Rev.* **24**, 81 (2003).

[2] F.J. Humphreys, M. Hatherly, *Recrystallization and Related Annealing Phenomena*, 2nd ed., Elsevier, Amsterdam 2004.

[3] A. Røyset, N. Ryum, *Int. Mater. Rev.* **50**, 19 (2005).

[4] H. Westengen, O. Reiso, L. Auran, *Aluminium* **12**, 768 (1980).

[5] J.D. Robson, P.B. Prangnell, *Acta Mater.* **49**, 599 (2001).

[6] Z. Jia, G. Hua, B. Forbord, J.K. Solberg, *Mater. Sci. Eng. A* **444**, 284 (2007).

[7] P. Kolby, C. Sigli, in: *Proc. 4th Int. Conf. on Aluminium Alloys (ICAA4), Atlanta (USA)*, Ed. T.H. Sanders, E.A. Starke, Georgia Institute of Technology, Atlanta 1994, p. 508.

[8] P.C.M. de Haan, J. van Rijkom, J.A.H. Søntgerath, *Mater. Sci. Forum* **217-222**, 765 (1996).

[9] J.D. Robson, *Mater. Sci. Eng. A* **338**, 219 (2002).

[10] Y.J. Li, L. Arnberg, *Acta Mater.* **51**, 3415 (2003).

[11] F. Nakamura, S. Hirosawa, T. Sato, in: *Proc. 9th Int. Conf. on Aluminium Alloys (ICAA9), Brisbane (Australia)*, Eds. J.F. Nie, A.J. Morton, B.C. Muddle, Institute of Materials Engineering Australasia Ltd, North Melbourne 2004, p. 582.

[12] Z. Jia, G. Hua, B. Forbord, J.K. Solberg, *Mater. Sci. Eng. A* **483-484**, 195 (2008).

[13] M. Karlík, M. Slámová, T. Mánik, *Kovové Materiály — Metallic Mater.* **47**, 139 (2009).

[14] M. Karlík, T. Mánik, H. Lauschmann, *J. Alloys Comp.* **515**, 108 (2012).

[15] E. Anselmino, A. Miroux, S. van der Zwaag, *Mater. Character.* **52**, 289 (2004).

[16] J. Ondráček, B.Sc. Thesis, Czech Technical University in Prague, Faculty of Nuclear Sciences and Physical Engineering, 2009 (in Czech).

[17] D.T.L. Alexander, A.L. Greer, *Acta Mater.* **50**, 2571 (2002).

[18] T. Sato, A. Kamio, W. Lorimer, *Mater. Sci. Forum* **217-222**, 895 (1996).

[19] N.A. Belov, A.N. Alabin, V.V. Istomin-Kastrovskiy, in Ref. [11], p. 1270.

[20] E.J. Westermann, in: *Aluminium Alloys for Packaging*, Eds. J.G. Morris, H.D. Merchant, E.J. Westermann, P.L. Morris, TMS, Warrendale (PA) 1993, p. 1.

[21] H. Cama, J. Worth, P.V. Evans, A. Bosland, J.M. Brown, in: *SP'97 Proc. 4th Decennial Int. Conf. on Solidification Processing*, Eds. J. Beech, H. Jones, University of Sheffield, Sheffield 1997, p. 3.

[22] M. Slámová, P. Sláma, M. Cieslar, *Mater. Sci. Forum* **519-521**, 365 (2006).

[23] M. Cieslar, M. Slámová, J. Uhlíř, Ch. Coupeau, J. Bonneville, *Kovové Materiály — Metallic Mater.* **45**, 91 (2007).

[24] Y.J. Li, L. Arnberg, *Mater. Sci. Eng. A* **347**, 130 (2003).

[25] Y.J. Li, L. Arnberg, *Mater. Sci. Forum* **396-402**, 875 (2002).